Structure, Selectivity, and Solvation of a Model Chiral Stationary Phase

S. Nita, N. M. Cann,* and J. H. Horton*

Department of Chemistry, Queen's University, Kingston, Ontario, Canada K7L 3N6

Received: August 28, 2003; In Final Form: January 9, 2004

The presence of chirality at an interface enables a surface to distinguish between enantiomers. The mechanism by which this selectivity occurs is complicated by the surface morphology, the possible involvement of the solvent, and the characteristics of the chiral molecules at the surface. In this article, atomic force microscopy (AFM), chemical force titrations, density functional theory, and molecular dynamics simulations are employed to examine surfaces terminated by (*S*)- and (*R*)-*N*-(1-phenylethyl)-*N*′-[3-(triethoxysilyl)propylurea (PEPU). A "brush-type" chiral interface is formed by attaching the PEPU molecules to either an oxidized poly(dimethylsiloxane) or oxidized Si(111) substrate. Using AFM, the morphologies of the resulting chiral surfaces are obtained. Chemical force measurements of the chiral selectivity in the presence of water, methanol, hexane, and CS_2 have been performed. Ab initio studies provide descriptions of the hydrogen bonding between PEPU molecules at the interface. Molecular dynamics simulations are employed to examine the distribution of water, methanol, and CS_2 near PEPU interfaces.

1. Introduction

The fundamental physical property at work in chiral chromatography (separations of chiral molecules) is the enantioselective interaction between a chiral selector and two mirror-image molecules. A chiral interface, or chiral stationary phase (CSP), is the usual mechanism for introduction of the selector, but chiral additives can also form part of the mobile phase. In a typical type I, or Pirkle,[1] CSP, a chiral molecule is attached, usually via some sort of amide or ether linker, to a "tether" molecule. The tether is then attached to the surface of a colloidal silicate particle via a siloxane linkage. While there has been an increase in commercially available CSPs, there has not been a commensurate growth in the molecular level understanding of the mechanisms by which they operate.[2,3] This understanding is crucial for the *systematic* development of new and improved CSPs and ultimately impacts our ability to separate enantiomers. This paper will address this lack of fundamental knowledge by examining the detailed atomic structure and dynamics at a type I chiral interface using molecular dynamics simulations, ab initio methods, and techniques in scanning probe microscopy, particularly chemical force methods.

The interface under consideration is (*S*)-/(*R*)-*N*-(1-phenylethyl)-*N*′-[3-(triethoxysilyl)propylurea] (Figure 1), or PEPU. The PEPU molecule has been used previously for chromatographic separation of isocyanate and isothiocyanate derivatives of (*S*)-/(*R*)-propranolol.[4,5] In particular, this interface was successful in separating several derivatives of propanolol, for which other related CSPs were unsuccessful. Interestingly, the elution order and enantiomeric resolution were not consistent with simple arguments of the π-basic character of the PEPU aromatic ring. The PEPU interface also contains many of the features common to type I CSPs: an alkyl tether to the surface, a chiral center, the presence of phenyl groups which may undergo π stacking interactions, and sites which may undergo hydrogen bonding in solution. Thus, we expect that many of the attributes of the PEPU interface should be transferable to other CSPs.

On a more practical level, we selected the PEPU molecule for several reasons. First, both enantiomers are commercially available in high purity. Second, it may be readily self-assembled on a flat, silanol (−SiOH) terminated surface, such as oxidized silicon or poly(dimethylsiloxane) (PDMS), through a hydrolysis reaction. In this way, we can readily synthesize a surface which is convenient for imaging by atomic force microscopy (AFM). Third, the mechanism of selection by PEPU, although complex, does not involve inclusion complexes, and each PEPU contains a single chiral center within the molecule. Finally, the relatively well-defined structure of the PEPU interface is amenable to molecular dynamics simulations.

There are several notable examples of chiral molecules studied on surfaces using scanning probe methods, particularly scanning tunneling microscopy. An early result was the identification of *R*,*R* and *S*,*S* isomers of *trans*-2-butene[6] on Si(100). This molecule is not intrinsically chiral, but becomes so when restricted in rotation on a two-dimensional surface. Other important efforts have focused on chiral molecules adsorbed on Cu or Au surfaces, such as tartaric acid on Cu(110),[7] cysteine on Au(111),[8,9] or glucose oxidase on modified Au surfaces.[10] Chemical force microscopy (CFM) provides a completely different approach to scanning probe research on chiral molecules. With CFM, the emphasis is placed on the measurement of chemical forces between two chiral surfaces, rather than the structure of a single surface with atomic resolution. The first application of CFM to chiral systems was the interaction of AFM tips derivatized by a Pirkle-type CSP (DNB-phenylglycine) with Au surfaces derivatized by mandelic acid.[11] The adhesive force between the tip and sample was found to vary by up to 1 nN when the two were of like stereochemistry (*R*/*R* or *S*/*S*) as opposed to unlike (*R*/*S* or *S*/*R*). It is this sort of CFM experiment which we will report on here, except that the CSP derivative is present on both tip *and* sample.

Techniques for atomistic modeling of chiral interfaces have been summarized in several recent reviews.[2,12−14] Briefly,

* To whom correspondence should be addressed: theoretical details, N.M.C.; experimental details, J.H.H. Telephone: (613) 533-2379, (613) 533-2651. Fax: (613) 533-6669. E-mail: hortonj@chem.queensu.ca (J.H.H.); ncann@chem.queensu.ca (N.M.C.).

10.1021/jp0365615 CCC: $27.50
Published on Web 02/21/2004

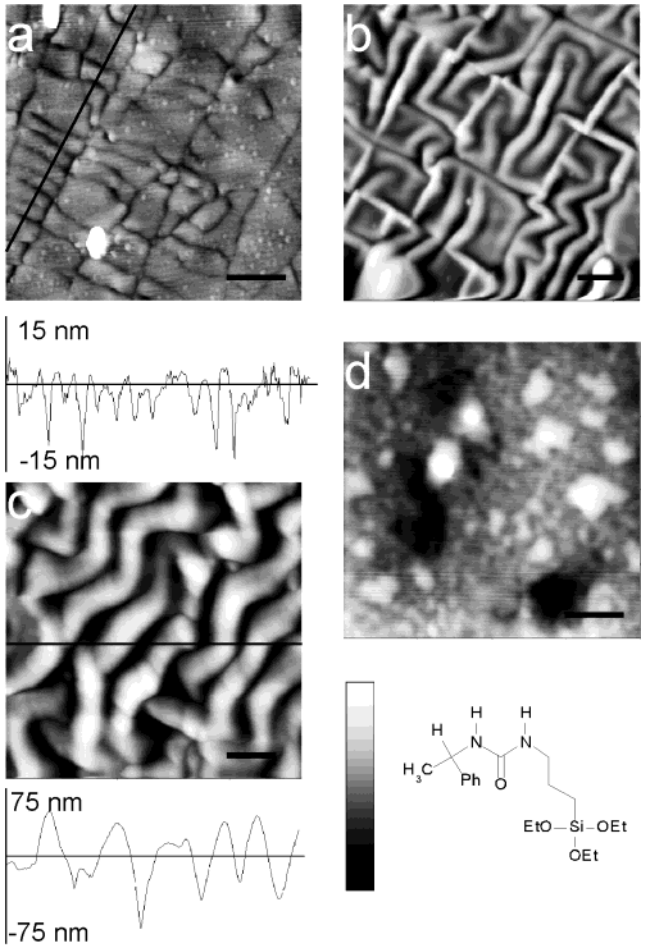

Figure 1. AFM images of the various surfaces under study. (a) PDMS surface after undergoing oxidation using a Tesla coil. Scale bar is 2 μm; vertical scale is 67 nm. (b) PDMS surface after exposure to PEPU. Scale bar is 1 μm; vertical scale is 250 nm. (c) As in (b) but scale bar is 400 nm; vertical scale is 100 nm. (d) Si(111) surface after exposure to PEPU. Scale bar is 2 μm; vertical scale is 50 nm. (e) As in (b) but scale bar is 500 nm and vertical scale is 20 nm. A diagram of the PEPU molecule is also shown in the figure.

modeling is generally restricted to ab initio or molecular mechanics calculations for noncovalently bonded host−guest complexes in the absence of solvent. The objective is to explore the role of hydrogen bonding, van der Waals forces, and charge transfer in the stable configurations of the two diastereomeric complexes (host−guest (*R*), host−guest (*S*)). The energetic differences between the diastereomeric pairs are typically several orders of magnitude smaller than the individual complexation energies. Hence, the approach is sensitive to details of the method and relies heavily upon a cancellation of errors. Such calculations have nonetheless proved valuable, particularly for gas-phase chiral chromatography where solvation is removed from consideration. Stationary phases that tend to form inclusion complexes are also amenable to this type of modeling, and recent work by Lipkowitz[15] on selection by cyclodextrin is particularly noteworthy. Recent emphasis[16−19] on comprehensive and automated search algorithms over the conformational space of the diastereomeric complexes has improved the accuracy of the predicted free energies for discrimination.

An entirely different approach to the prediction of selectivity by CSPs invokes statistical modeling. The objective is to obtain quantitative structure−function relationships[20,21] that are direct analogues of the more well-known structure−activity relationships (QSAR[2]) often used in drug design. In the end, experimental results for a series of analytes are expressed as a function of molecular descriptors and sophisticated regression is performed. The objective is to arrive at a compact set of descriptors that reproduce experimental results (elution order, enantioseparation factor) and have predictive power for related analytes. At some implicit level, a representation of the CSP and solvent is included in this approach. However, in practice, a physical picture of the enantioselection process cannot be extracted from the final set of descriptors.

In liquid, subcritical, or supercritical chromatography, the solvent actively participates in the enantioselection process.[22] Typical solvents[23] are mixed and predominantly apolar, but deviations from this prescription are numerous. The choice of solvent is critical, yet little is known about the details of the solvent distribution around the CSP or the analyte.[2] In this article, molecular dynamics simulations of the PEPU interface are performed in the presence of three solvents: water, methanol, and carbon disulfide. These solvents are chosen since they provide a clear picture of the affinity of polar vs apolar solvents for the PEPU interface. Also, the comparison between water and methanol provides insights into the impact and prevalence of solvent hydrogen bonding at the PEPU surface.

Several chiral interfaces have been examined, beginning with a perfectly regular surface, and proceeding to include a series of surface imperfections. Molecular dynamics simulations of the interface require an atomic level description of the PEPU molecules. A realistic model interface has been constructed based on a series of density functional theory calculations[24] for PEPU monomers, dimers, and solvated clusters. In particular, the relative distribution of pairs of PEPU molecules has been explored in considerable detail: Intertether separation and hydrogen bonding, along with $\pi-\pi$ stacking and relative headgroup orientation between PEPU molecules, have been examined. A hydrogen bonding solvent, such as water or methanol, could also hydrogen bond with the urea segment of the tether. The presence of solvent among the tethers places structural restrictions on the rest of the molecule. As well, hydrogen bonding and π stacking between adjacent PEPU molecules may be disrupted by solvent in the tether region. We explore the consequences of water, hydronium, and hydroxide ions present within the tether regions.

A detailed exploration of structure, solvation, and selectivity of the PEPU interface is presented in this article. Brief descriptions of the experimental and computational methods are given in section 2. Our results are presented in section 3. The paper concludes with a brief summary in section 4.

2. Experimental and Computational Methods

2.1. Sample Preparation and AFM Measurements. Two different substrates—oxidized poly(dimethylsiloxane) (PDMS) and Si(111)—were used for deposition of PEPU. These were examined under three different solvents: aqueous solutions of varying pH, methanol, and CS_2. All glassware used in chemical modification of either the substrate or AFM tips was passivated toward adsorption of alkoxysilanes. This was carried out by exposing the glassware to a 10^{-3} mol L^{-1} solution of octadecyltrichlorosilane in toluene. The AFM tips used in the chemical force titration measurements were standard silicon nitride cantilevers (Digital Instruments, Santa Barbara, CA). The tips were cleaned in deionized water and then methanol prior to the PEPU modification. These were functionalized with a chirally terminated surface by immersing the entire tip and cantilever assembly in a solution of 1.0×10^{-3} mol L^{-1} in toluene of either (*R*)- or (*S*)-*N*-(1-phenylethyl)-*N*′-[3-(triethoxysilyl)propylurea] (95%, Gelest Inc., Tullytown, PA) for 24 h.

The first substrate used was based on a PDMS formulation (Sylgard 184 silicone elastomer and curing agent in a 10:1 mass ratio, Dow Corning Corporation, Midland, MI). The PDMS polymer mixture was poured into a glass Petri dish and allowed to cure at 65 °C for 4 h, to form a layer roughly 1 mm thick. The surface of these resulting PDMS samples were flat and essentially featureless, as determined with AFM imaging. The PDMS samples were further modified to form an oxidized surface. Oxidation was carried out by ozonolyis with the ozone generated by the electrical arc discharge of a Tesla coil. The PDMS sample was placed on a stainless steel plate within a fume hood. A Tesla coil was placed at a distance of 1−2 cm from the PDMS surface to produce an electrical arc, and the treatment was carried out for approximately 10 min. Following oxidation, the originally hydrophobic surface of the PDMS was easily wetted with water. AFM and CFM studies of such samples have shown that they are indeed terminated with SiOH sites.[25,26] These oxidized samples were either used immediately to provide a control surface in chemical force experiments, or further treated to produce a chirally modified sample by immersing the oxidized PDMS in a solution of 1.0×10^{-3} mol L^{-1} in toluene of either (*R*)- or (*S*)-*N*-(1-phenylethyl)-*N*′-[3-(triethoxysilyl)propylurea] for 24 h. In this reaction, the ethoxysilane group of PEPU undergoes hydrolysis to form an Si−O linkage directly to surface siloxy sites.

The second substrate was an oxidized Si(111) surface. The Si wafers were etched based on the method described by Hines.[27] Prior to etching, the glassware was cleaned using a basic peroxide solution composed of 1:1:4 volumes of 28% $NH_{3(aq)}$:30% $H_2O_{2(aq)}$:H_2O at 80 °C for 10 min and then rinsed with doubly deionized distilled water. The Si samples were cleaned in the basic peroxide solution described above for 10 min, and after this the oxide layer was stripped by immersion in an aqueous $HF_{(aq)}/NH_4F_{(aq)}$ solution for 2 min. After thorough rinsing, the samples were cleaned once again using 1:1:4 volumes of 30% $HCl_{(aq)}$:30% $H_2O_{2(aq)}$:H_2O at 80 °C for 10 min and then rinsed with doubly deionized distilled water. PEPU was deposited by immersing the samples into a solution of PEPU in dry toluene for 30 min, within a glovebox.

AFM data were acquired using a PicoSPM (Molecular Imaging, Tempe, AZ), using a Nanoscope IIE controller (Digital Instruments, Santa Barbara, CA). Images were acquired under ambient conditions, using the magnetic A/C (i.e., intermittent contact) mode. The magnetically coated cantilevers used for image acquisition were terminated with standard Si_3N_4 tips and had a resonance frequency of ∼100 kHz. Height and phase shift data were recorded simultaneously, although only the height mode images are shown here. Images were recorded at scan rates of 1−2 Hz using a 30 μm × 30 μm scanner.

CFM data were obtained using the same apparatus. For the acquisition of force-displacement curves, a chemically modified tip and corresponding sample were immersed in the appropriate solvent. In the case of experiments carried out in aqueous solution, freshly prepared unbuffered NaOH or HCl solutions of pH ranging from 3 to 10 were used. The pH of the solutions was checked before and after the experimental run to ensure that the pH had not changed. A series of 300−500 force curves was obtained at 10 locations on each sample surface for each sample−tip combination. The average values of the adhesive interaction are reported while the errors reflect the standard deviation of the data. The force constants of the AFM tips used here were calibrated (following chemical modification) using the method of Hutter and Bechhoefer,[28] and ranged from about 0.2 to 1.0 N m^{-1}.

2.2. Ab Initio Calculations and Molecular Dynamics Simulations. Ab initio calculations were performed on slightly modified PEPU molecules. In particular, the representation of the triethoxysilyl group, which covalently attaches the tether to the surface, is somewhat problematic. First, the method of attachment of the triethoxysilyl to the surface is complex, with the possibility of intertether linkages, as well as direct attachment to the surface. Second, the group is large and "far" from the chiral center. We have proceeded by replacing the triethoxysilyl group with a hydrogen, which terminates the tether by a methyl group. To reproduce the physical constraints of the surface, the distance between two hydrogens on the terminal methyls of two PEPU molecules is constrained to correspond to a typical[29,30] Si−O−Si distance, 3 Å.

Geometry optimizations have been performed for PEPU monomers, dimers, and dimers in the presence of water and ions. The 6-31G* basis set and density functional theory, with the B3LYP[31] functional, are employed for these calculations. Following the optimizations, single point calculations are performed with the 6-311++G** basis set to provide a better estimation of the relative energies for the minima. In particular, greater flexibility in the representation of hydrogen is desirable because of the prevalence of hydrogen bonding in these complexes. Each ab initio calculation is repeated 3−5 times starting from different initial configurations to identify the most important minimum energy configurations. The Gaussian 98 program,[22] run in parallel over eight nodes, was employed for all ab initio calculations. Each geometry optimization requires between 4 and 10 days on a Sun Fire 6800.

The impact of implicit solvent was explored for the PEPU monomer, which was surrounded by a dielectric continuum of $\epsilon = 87.3$ D, typical for water. The geometry of the solvated molecule was optimized with the SCI-PCM (self-consistent isodensity polarized continuum model) method,[32] but was quite similar to that of the isolated monomer. Given the small changes observed for water, implicit methanol and CS_2 were not considered. In the description of the PEPU interface, explicit solvent is more pertinent. First, only a portion of the PEPU molecule is exposed to solvent. Second, hydrogen bonding between solvent and PEPU requires explicit solvent. Conformations of solvated PEPU dimers, with zero to four water molecules in the tether region, have been obtained. The presence of hydronium or hydroxide ions between the tethers has also been considered.

Model chiral stationary phases for PEPU are constructed based on the ab initio results, and with the mesostructure of the PDMS and silicon surfaces in mind. To study the effects of surface characteristics, interfaces with imperfections have been examined along with the ideal surface of ordered PEPU molecules. The "perfect" surface has been constructed from the optimized PEPU monomer with the terminal hydrogens used in the ab initio calculations replaced by silicon atoms. Imperfections consist of single molecule holes, five molecule cross-shaped holes, and a row of missing PEPU molecules. The PEPU molecules interact with the solvent through Lennard-Jones and electrostatic potentials. CHARMM[33] parameters are employed for the former, but atomic charges extracted from Mulliken population analysis of the optimized monomer are employed for the latter. The united-atom representation, where the hydrogens do not appear explicitly, is used throughout. Details of the PEPU model, as employed in the simulations, are given in Table 1. In total, four selective interfaces were explored, and each surface consisted of 1088−1700 atoms.

TABLE 1: Details of the PEPU Monomer Model[a]

atom	ϵ (kJ/mol)	σ (nm)	q ($\|e\|$)	x (nm)	y (nm)	z (nm)
CH_2 (terminal)	0.477 81	0.2235	0.005 496	−0.176	0.789	0.672
CH_2	0.477 81	0.2235	−0.012 318	−0.139	0.404	2.098
CH_2	0.477 81	0.2235	0.152 826	−0.037	1.588	2.971
NH	0.997 46	0.1600	−0.142 602	−0.351	1.359	4.329
O	0.665 67	0.1600	−0.505 865	1.229	2.547	5.126
C	0.502 08	0.2100	0.526 152	0.250	1.977	5.333
NH	0.997 46	0.1600	−0.154 374	−0.228	1.956	6.573
CH_3	0.757 72	0.2165	0.020 026	0.092	4.056	7.840
CH (chiral)	0.203 34	0.2365	0.137 784	0.466	2.577	7.701
CH (phenyl)	0.502 08	0.2100	0.075 069	0.240	1.732	8.949
CH (phenyl)	0.502 08	0.2100	−0.048 216	−0.607	2.120	9.985
CH (phenyl)	0.502 08	0.2100	−0.022 550	0.899	0.503	9.057
CH (phenyl)	0.502 08	0.2100	−0.018 984	0.716	−0.313	10.164
CH (phenyl)	0.502 08	0.2100	−0.023 431	−0.795	1.303	11.098
CH (phenyl)	0.502 08	0.2100	0.010 987	−0.135	0.085	11.192

[a] CHARMM parameters have been adopted for short-ranged repulsion and dispersion (as described by ϵ and σ). The charges are given in units of e, the electron charge, and are obtained from Mulliken population analysis. The positions given in the last three columns are relative to a silicon atom at (0,0,0).

Extensive molecular dynamics (MD) simulations have been performed for the PEPU interface in the presence of three solvents: water, methanol, and CS_2. The extended simple point charge model (SPC/E) for water[34] has been employed, the Tildesley−Madden[35] model for CS_2 has been chosen, and Jorgensen's methanol model[36] has been used. The simulations are performed at 298 K and at the respective experimental densities. Each MD simulation follows the evolution of the interface for 100 000 time steps, with each step corresponding to 25 fs. A Nosé−Hoover thermostat[37] is used to generate canonical (NVT) averages. The initial configuration is obtained by placing a large number of fluid molecules on a regular lattice between the two surfaces. Then, molecules are removed at random until the desired number remain. Following this, a modest number of Monte Carlo cycles are performed to further randomize the starting configuration and eliminate any overlaps that may have been caused by the overly dense starting configuration. Finally, the molecules are assigned random linear and angular velocities consistent with the temperature, 298 K.

The solvents are confined between two surfaces, as is often done[38] for simulations of interfaces, so that three-dimensional (3D) boundary conditions can be applied. Each surface consists of PEPU monomers attached to two layers of underlying silicon arranged in a hexagonal array with a silicon−silicon distance of 3 Å. The surfaces, including the silicon atoms, are roughly 14.6 Å thick and are positioned perpendicular to the z-axis of the cell. Our simulation cell is a rectangular prism, and the full cell consists of a slab (500 solvent molecules between two PEPU surfaces) with empty space in the z-direction, above and below the surfaces. The inclusion of empty space is necessary to eliminate any interactions between slabs. For water, the dimensions of the cell are 24 Å × 24 Å × 120 Å with an intersurface (between silicon atoms on the upper and lower surfaces) distance of 55.143 Å. The corresponding dimensions are 30 Å × 30 Å × 150 Å with an intersurface distance of 66.5 Å, and 30 Å × 30 Å × 200 Å with surface separation of 84.9 Å, for methanol and CS_2, respectively. The intersurface distance is chosen such that fluid at the very center of the full simulation cell has bulk density and does not show surface-induced structure. In practice, we require that the distance between the center of the simulation cell and the topmost carbon of the PEPU molecule exceeds four solvent diameters. In this way, molecules at the center of the cell are at least four solvent diameters away from any surface. Water is the most dense of the three solvents, and we confine the fluid between two surfaces with 64 PEPU molecules (8 × 8) each. With this size surface, an intersurface distance of 55.143 Å is chosen so that bulk water density is recovered between the plates and the distance between the topmost carbons (roughly 25.9 Å) exceeds the minimum of eight solvent diameters. Methanol and CS_2 are less dense than water and simulation cells with 100 PEPU surfaces (10 × 10) were feasible for 500 solvent molecules.

The representation of interfaces in a simulation is complicated by the required periodicity of the simulation cell. In this article, 3D periodicity is applied with Ewald[39] summations used to treat the long-ranged Coulombic forces between charged sites. Although Ewald summations substantially lengthen the simulation time, there is now considerable evidence[34] that alternatives which truncate the long-ranged forces introduce significant errors. This may be particularly important for CSPs that include hydrogen bonding regions. The Ewald sums include a correction[40] for the shape of the simulation cell. Yeh and Berkowitz[41] have recently shown that the inclusion of this shape correction is essential in the application of 3D Ewald summations for systems with a slab geometry. In particular, two-dimensional results are recovered provided the simulation cell includes enough empty space above and below the two surfaces. Our simulation cell is 5−7 times longer in the z-direction than along the x- and y-axes. On the other hand, the intersurface distance is 2−3 times the side length of the cell. The remaining empty space is sufficient to eliminate interactions between slabs, provided that the Ewald sum appropriate for rectangular prisms is applied. All results below correspond to a position space cutoff of $\alpha L_x = 7.175$, and a momentum space cutoff of $k^2 = 27.0/L_x^2$.

3. Results and Discussion

3.1. Morphology of the PEPU Interface. PEPU was deposited onto two different substrates in order to model the "brush type" structures found on colloidal silica particles in chiral stationary phases and to explore the impact of larger scale structure on selectivity. Of the various systems discussed below, it should be noted that the PEPU-modified Si(111) surface in methanol showed the best evidence of chiral discrimination, although the other systems under study also provide insights into the nature of chiral discrimination at surfaces. We will begin by discussing the PDMS surface which had undergone plasma oxidation using a Tesla coil. An AFM image of the oxidized PDMS is shown in Figure 1a. While the original PDMS surface is essentially featureless, Figure 1a demonstrates that upon oxidation new features form, including channel structures which

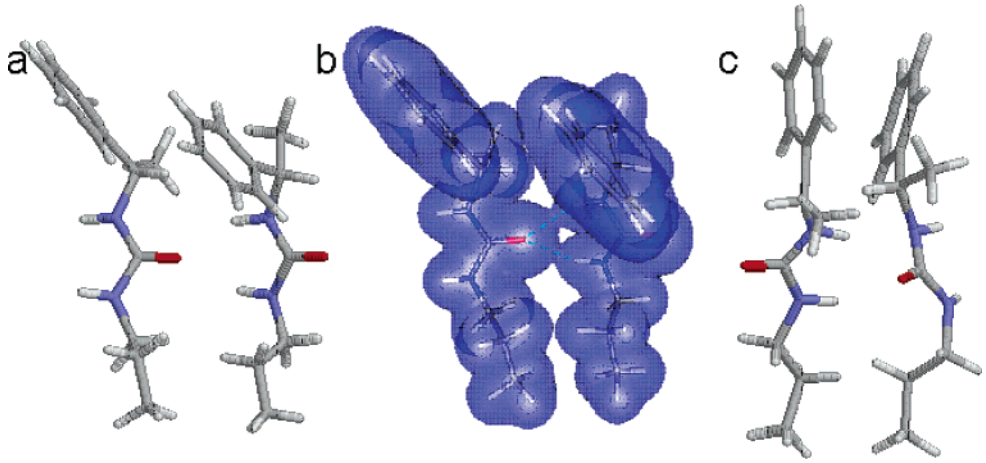

Figure 2. Structure of two PEPU dimers, $(PEPU)_2$, with the distance between two terminal hydrogens constrained to 3 Å. The lowest energy structure is shown in (a) with the corresponding electron density (0.01 contour level) given in (b). For the structure shown in (c), the distance between the chiral carbons is also constrained to 3 Å. The oxygen, nitrogen, carbon, and hydrogen atoms are indicated in red, blue, gray, and white, respectively.

can be several micrometers long. Previous work, using both X-ray photoelectron spectroscopy[42] and chemical force titration,[26] have shown that upon oxidation the surface becomes terminated with SiOH sites. These channels may indicate small regions of relatively unreacted hydrophobic PDMS, especially considered in light of the observations on the surface exposed to PEPU, described below. In any case, the resulting SiOH sites on the surface can be subsequently reacted with the ethoxy groups of PEPU to form a covalent link to the surface:

$$-\mathrm{Si}-\mathrm{OH} + (\mathrm{C_2H_5O})_3\mathrm{Si}-\mathrm{PEPU} \rightarrow -\mathrm{Si}-\mathrm{O}-(\mathrm{C_2H_5O})_2\mathrm{Si}-\mathrm{PEPU} + \mathrm{C_2H_5OH} \quad (1)$$

leaving two more ethoxy groups which might undergo further links to the surface or, more likely, react with ethoxy groups on neighboring PEPU molecules and those in solution to form a cross-linked structure. As seen in Figure 1b, and in the higher resolution Figure 1c, the resulting PEPU-terminated surface consists of long twisted ridge structures. These structures are as much as 1 μm in diameter and 150 nm in height and themselves contain some finer structure. A comparison of the cross sections between the oxidized (Figure 1a) and PEPU-modified (Figure 1b) surfaces indicate that, during PEPU deposition, a multilayer of material has been deposited on the surface. However, the more interesting observation in Figure 1b is a still larger scale structure. The ridges are assembled into square-shaped domains on the surface. The size and shape of these square domains is similar to that of the regions bound by the channels on the original oxidized surface, indicating that the original surface structure has templated the growth of the overlying PEPU layer. We have observed similar-looking structures, although without as good evidence for the large-scale templating, for surfaces terminated with (aminopropyl)-triethoxysilane, $(CH_3CH_2O)_3Si(C_3H_6)NH_2$.[26] Using 4-[*N*,*N*-(2-pyridyl)aniline]triethoxysilane, a molecule with an extensive π system, also gives a similar structure with much stronger templating features. Recently,[43] other workers have reported on the templating of triethoxysilanes on indium−tin oxide substrates, although in this case the underlying substrate contained long grooves, leading to a highly aligned overlayer. Again, they found that triethoxysilanes containing larger π systems tended to form more ordered structures. These observations show that the large-scale templating of triethoxysilanes on substrates is a fairly universal trend. π stacking interactions may also play a role in determining the degree of ordering in these structures. However, as outlined in section 3.2, ab initio calculations on PEPU dimers suggest that hydrogen bonding between the urea groups is more important in this system.

While the modified PDMS surface contains some interesting features, the complex morphology proved to be an impediment to chemical force measurements on the surface, as seen in section 3.4. Therefore, we also tried modifying an oxidized Si(111) surface with a layer of PEPU, again through a covalent Si−O linkage. The deposition of alkoxylsilanes and chlorosilanes on Si surfaces has been extensively studied.[44] AFM images of the PEPU-terminated Si surface are shown in Figure 1d,e. Several pits, probably a result of the Si etch process, as well as some agglomerates, presumably of highly cross-linked PEPU, are present on the surface, but generally, it is much smoother than the modified PDMS layer. This is shown by a direct comparison of the root-mean-square roughness of the two surfaces. The roughness of the modified PDMS layer is 23 ± 3 as compared to 8.2 ± 0.7 nm for the modified Si surface.

3.2. Atomic Structure of the PEPU Interface. PEPU molecules form self-assembled monolayers at the Si(111) surface and on PDMS. To understand the impetus driving this assembly, and to obtain an atomic level description for the surface, we undertook a detailed ab initio study of PEPU molecules. We focused primarily on pairs, or dimers, of PEPU molecules. The distance between two terminal hydrogens (which replace the silicon atoms and terminate the chains) of the tethers is constrained to 3 Å in these calculations to reproduce the effect of the siloxane connection. The optimized dimer structure is shown in Figure 2a. It is immediately obvious from the figure that the urea segments have aligned for hydrogen bonding. This is accomplished by a slight compression of one PEPU molecule placing its carbonyl oxygen between two hydrogens from the neighboring molecule. Despite the compression, the urea segments constrain the tethers into rough alignment. The two PEPU molecules are well positioned for further hydrogen bonds to other molecules.

$\pi-\pi$ attractive interactions have very little influence on the structure of the PEPU dimer. This is evident from Figure 2a, where the distance between ring centers is 5.78 Å, which is too large for significant interaction between the rings. Further evidence for this is provided in Figure 2b, where the electron density is shown. Electron density within the hydrogen bonding region of the tethers is evident, but at this contour level, there

TABLE 2: Selection of ab Initio Energies for PEPU Monomers, Dimers, and Solvated Dimers[a]

cluster	6-311++G** energy (a.u.)	relative energy[b] (kJ/mol)	relative energy[c] (kJ/mol)	phenyl distance (nm)	phenyl angle (deg)
PEPU	−653.0490				
$(PEPU)_2$	−1306.1060	−20.87		0.578	11.83
$(PEPU)_2$[d]	−1306.0869	29.20		0.383	17.73
$(PEPU)_2$[e]	−1306.1024	−11.81		0.767	43.02
$(PEPU)_2\cdot(H_2O)$	−1382.5743	−46.89	−26.02	0.729	32.01
$(PEPU)_2\cdot(H_2O)_2$	−1459.0436	−75.41	−37.65	0.713	37.89
$(PEPU)_2\cdot(H_2O)_3$	−1535.5128	−51.68	−16.81	0.713	37.89
$(PEPU)_2\cdot(H_2O)_4$	−1611.9933	−161.70	−22.87	0.892	19.45
$(PEPU)_2\cdot(H_2O)_4$	−1611.9831	−135.02	−17.12	0.511	66.31
$(PEPU)_2\cdot(H_3O^+)$	−1382.9592	−341.81	−320.94	0.581	75.28
$(PEPU)_2\cdot(H_2O)_2(H_3O^+)$	−1535.8947	−390.74	−115.92	0.923	30.61
$(PEPU)_2\cdot(H_2O)_2(H_3O^+)$	−1535.9048	−417.39	−142.58	0.756	47.80
$(PEPU)_2\cdot(OH^-)$	−1382.0395	−300.35	−279.48	0.729	73.20
$(PEPU)_2\cdot(H_2O)_2(OH^-)$	−1534.9803	−363.25	−136.37	1.271	85.73
$(PEPU)_2\cdot(H_2O)_2(OH^-)$	−1534.9475	−277.19	−50.31	0.547	59.06

[a] Geometries are optimized with the B3LYP functional and the 6-31G* basis set. Single point calculations, with the 6-311++G** basis set, are performed at these geometries. Relative energies are obtained by comparison with the relevant isolated molecules, or molecular clusters, optimized at the same level of theory. All structures are minimized subject to the constraint that the terminal hydrogens are 3 Å apart. [b] Energy relative to isolated PEPU, water, and ions. [c] Energy relative to $(PEPU)_2$ and water, or solvated ion, cluster. [d] The chiral carbon−chiral carbon distance is also constrained to 3 Å. [e] Energy of $(PEPU)_2$ configuration that places the phenyls in a roughly staggered configuration.

is no density between the phenyls. Although the inter-ring distance is large, the phenyls are approximately eclipsed and form a roughly 110° angle with the tether. This arrangement leaves the chiral centers exposed at the top of the chain.

The robustness of the alignment of PEPU molecules was tested in three ways. First, the distance between the tethers was varied between 2.5 and 4 Å. We have concluded from these calculations that the PEPU molecules are too close at 2.5 Å, and that 4 Å is a rough maximum beyond which the hydrogen bonding interactions are too weak to align the tethers. A second test is provided by constraining the distance between the chiral carbons. When this distance is 3 Å, the structure in Figure 2c is obtained. It is clear that hydrogen bonding between the PEPU molecules has been eliminated and the overall alignment of the tethers is poor. The energy of this doubly constrained dimer is substantially higher than the dimer in which only the terminal hydrogens are constrained (Table 2). In fact, the energy of the doubly constrained dimer is higher than the energy for two isolated monomers. This is not the case for the dimer in Figure 2a, where the hydrogen bonding between the tethers lowers the energy relative to the monomers. As a final test, the relative orientation of the PEPU molecules was varied in the initial geometry. One optimized conformation, in which the phenyls are staggered, is listed in Table 2. This configuration is less stable than the dimer in Figure 2a. Together, these results suggest that hydrogen bonding is primarily responsible for stabilizing the self-assembled PEPU, that self-assembled layers will form preferentially on surfaces that can place the tethers at 3−4 Å, that the degree of alignment between the tethers is high, and that the phenyl groups will be roughly eclipsed.

The presence of solvent within the CSP could dramatically alter the relative orientation of the chains. For PEPU, the impact of solvent is particularly difficult to predict. A polar solvent will avoid the phenyl groups but could hydrogen bond with the urea segments of the tethers. An apolar solvent is expected to prefer the topmost portion of the CSP, leaving the intertether structure intact. Thus, we expect that water and, to a lesser extent, methanol may be present within the tethers. This interaction with the chains could disrupt the intertether alignment. The overall impact of solvent may be more pronounced on the PDMS surface where the surface morphology exposes more tethers.

To explore the impact of solvent amid the tethers, we have performed a series of ab initio calculations on PEPU dimers with water. Specifically, the energy change for the following process has been evaluated:

$$(PEPU)_2 + (H_2O)_n \rightarrow (PEPU)_2\cdot(H_2O)_n \qquad n = 1-4 \quad (2)$$

where the water molecules are initially placed near the hydrogen bonding regions of the tethers. Geometry optimizations have been performed for clusters with up to six molecules. In all cases, the intertether distance increases with the presence of the water. As expected, energy minimization identifies several stable configurations of the molecules. Figure 3 shows the extensive hydrogen bonding network that forms for two configurations of $(PEPU)_2\cdot(H_2O)_4$. In Figure 3a the intertether hydrogen bonding is largely intact but the chain alignment is poor. In Figure 3b, the water actively hydrogen bonds with the chains, greatly disrupting the chain alignment and leading to a distance of 8.9 Å between the center of the rings. Relative energies for the process (2) are given in Table 2 for several hydrated clusters. The relative energies are roughly −20 kJ/mol, indicating that the cluster is energetically favored. However, the impact of steric constraints from other neighboring PEPU molecules has not been included in these energies. We have seen above that simply constraining the chiral carbons to 3 Å resulted in a 50 kJ/mol increase in energy. Thus we conclude that water will not enter the tethers in a dense arrangement of PEPU molecules, but will interact with the tethers if space allows.

Chemical force microscopy measurements have been performed over a range of pH, as discussed in section 3.3. The impact of hydronium ions and hydroxide ions has also been examined with the processes

$$(PEPU)_2 + OH^-(H_2O)_n \rightarrow (PEPU)_2\cdot(OH^-)(H_2O)_n \qquad n = 0-3 \quad (3)$$

$$(PEPU)_2 + H_3O^+(H_2O)_n \rightarrow (PEPU)_2\cdot(H_3O^+)(H_2O)_n \qquad n = 0-3 \quad (4)$$

and the relative energies are given in the fourth column of Table 2. In all cases, the energy of the full cluster is lower than the

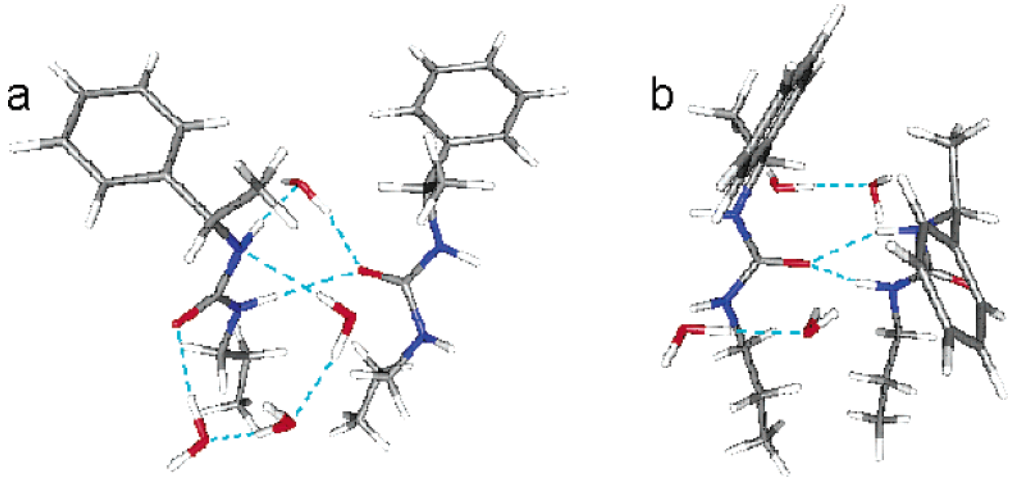

Figure 3. Two configurations for PEPU dimers when surrounded by four water molecules. See Figure 2 for the color identification of the atoms. The light blue lines indicate the location of hydrogen bonds. In (b) the hydrogen bonding between the PEPU is left largely intact while the water interferes with the PEPU hydrogen bonding in (a).

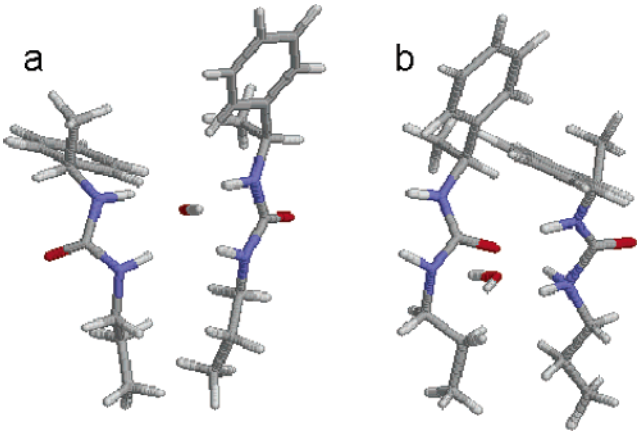

Figure 4. Impact of hydroxide (a) and hydronium (b) ions on $(PEPU)_2$. See Figure 2 for the color identification of the atoms.

energy for the isolated dimer and solvated ions. However, the energy drops as the number of waters surrounding the ion increases (n increases from 0 to 3). Structures for $(PEPU)_2 \cdot (OH^-)$ and $(PEPU)_2 \cdot (H_3O^+)$ are given in Figure 4. Although water has not been included in the structures shown, similar results are obtained in the presence of water. In Figure 4a, one of the PEPU molecules has been protonated by the hydronium ion. We find that, in these clusters, hydronium ions always protonate one of the nitrogens of the chain. The protonated chain then adopts a twisted structure that destroys the roughly eclipsed arrangement of the phenyl rings. Similarly, some of the geometry optimizations for hydroxide ions predict deprotonation at one of the nitrogens. When deprotonation occurs, the alignment of the chains decreases. However, as shown in Figure 4b, when the hydroxide ion remains intact, one of the PEPU chains rotates to provide strong hydrogen bonding between the ion and both tethers. In the surface environment, this type of rotation would be highly unfavored since it would destroy hydrogen bonding with neighboring PEPU molecules. We should note, however, that the pK_a values for protonation and deprotonation of urea are 0.1 and 35, respectively. Evidently, the presence of a neighboring PEPU molecule and aromatic rings within each molecule serves to stabilize a charged tether. However, as with the incorporation of water within the chains, the effects of surrounding PEPU molecules have not been accounted for. Once these effects are included, and factoring in that the energy is still increasing for $n = 3$ in (3) and (4), it is unlikely that protonation, or deprotonation, occurs within a dense array of PEPU molecules.

In summary, the ab initio results discussed above show that self-assembled PEPU molecules interact mainly by means of hydrogen bonding between the urea groups: the presence of water, hydroxide, or hydronium ions between the tethers increases the intertether distance and disrupts the crucial intertether hydrogen bonding. These results suggest that even polar solvents may be excluded, to a large extent, from between molecules in the CSP. We expect this to hold particularly true for PEPU layers deposited on the Si(111) surface. On the other hand, the morphology of the PDMS surface, with its numerous ridge and valley features (Figure 1b), suggests that there might be localized tether−solvent interactions. Only a small fraction of the overall surface area is positioned near a ridge or valley feature, however, so the overall solvent−tether interaction should be negligible on PDMS. It is worth noting that the radius of curvature of the AFM tip is large enough that the average distance between phenyls on neighboring PEPU molecules is only marginally larger than the distance between the terminal carbons of the tethers. Thus, the arrangement of PEPU molecules on the tip and sample will be nearly identical.

3.3. Solvation of the PEPU Interface. The solvation of the CSP directly impacts on the selectivity of the surface. For instance, a solvent that associates strongly can exclude enantiomers from the CSP. We have explored the dynamics of the solvent−CSP interaction for water, methanol, and CS_2. The latter is apolar and one expects that this solvent will strongly prefer the accessible and apolar phenyl regions of the PEPU molecules. The interaction of water or methanol with the CSP is substantially more complex. For instance, water is known to form a highly structured surface layer near uncharged surfaces with four- and five-membered rings evident.[36] For water, the poor interaction of the surface is offset by the energetic gains from an extensive hydrogen bonding network near the surface. For the PEPU interface, the presence of the urea group within the tether could potentially bring the water or methanol into closer proximity with the surface.

The distribution of water near the idealized CSP is shown in Figure 5. The side view of the simulation cell shows that the water is in contact with the surface and a higher solvent density is evident at the interface. Figure 5a also shows a well-defined second layer of water near the surface. Two snapshots of the water layer nearest the surface are shown in Figure 5b,c.

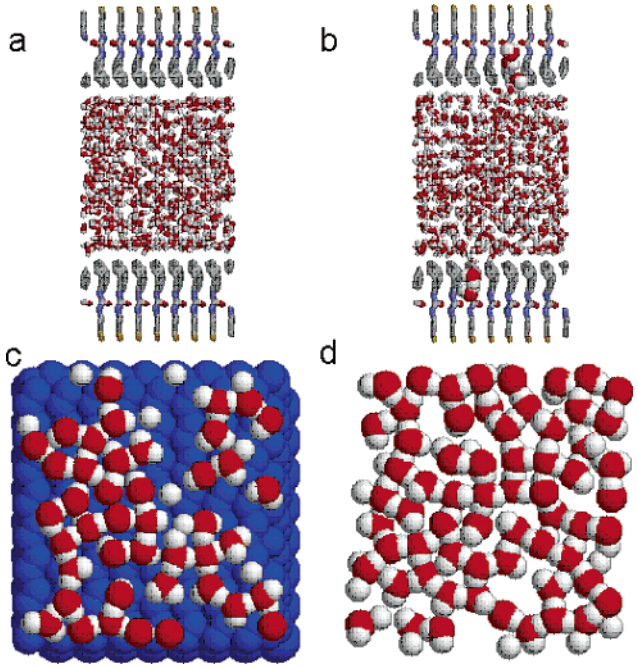

Figure 5. Snapshots from the simulations of water between two PEPU surfaces. Side views of the entire slab are shown in (a) and (b). The surfaces in (b) have imperfections in the form of five missing PEPU molecules in a cross shape. A snapshot of the contact layer (0−3 Å) is shown in (c). The second solvation layer (3−6 Å above the surface) is provided in (d). Oxygen and hydrogen atoms are red and white, respectively. In (c), the atomic positions of the underlying surface are shown in blue.

Extensive hydrogen bonding networks, and four- and five-membered rings, are evident. These ring structures have been noted previously, but only with respect to highly idealized surfaces. Evidently, the morphology of the PEPU surface also allows formation of the ring structures. A snapshot of the second surface layer is presented in Figure 5d. Here the hydrogen bonding network is still present but less pronounced. These simulations suggest that both the surface and the tip will be surrounded by two well-organized layers of water in a CFM experiment with PEPU. These layers will be perturbed when the tip and surface come together and also when they are pulled apart.

The distribution of water near imperfect PEPU surfaces has also been examined. The imperfections consist of single missing PEPU molecule, a row of missing molecules, or five missing PEPU molecules in a cross shape. In all cases, the PEPU molecules are no more than 8.5 Å apart across these relatively small holes. One or two water molecules enter into the larger holes and hydrogen bond with the urea segments (Figure 5b). Water also descends into the opening of the larger holes. However, the surface water layer near the imperfect surfaces is close to the structure near the perfect surface. Evidently, water maintains its stable hydrogen bonding network near small vacancies.

The distribution of methanol near the PEPU surface is shown in Figure 6. The side view of the interface shows a dense layer of methanol near the surface, but a second layer is only weakly present. A methanol monolayer is shown in Figure 6b. Here it is clear that methanol adopts a dramatically different structure from water. First, since the methyl groups do not hydrogen bond, ring structures cannot form at the interface. Second, the methanol layer is less dense than for water even though hydrogen bonds are present within the layer.

Figure 6c shows a side view of the methanol−PEPU interface when the surface has a row of missing molecules. The simulations of methanol near imperfect surfaces show that a few molecules do move to fill the surface vacancy. Specifically, depending of the size of the vacancy, molecules will descend into the opening while maintaining some contact with the surface layer above. These molecules are able to hydrogen bond with the upper layer and with each other. Over the time scale of the simulations, individual methanol molecules did not fully descend into vacancies in the surface but always maintained some contact with the surface layer.

An apolar molecule, such as CS_2, is expected to display a different distribution with the surface than polar, hydrogen bonding, solvents such as methanol or water. The simulations of the CS_2−PEPU interface show a dense layer of CS_2 near the surface (Figure 7) with the solvent preferring to point a sulfur atom toward the surface. Despite this preference, a small fraction of the CS_2 molecules lie flat on the surface. CS_2 responds to the presence of vacancies in the surface by moving into the

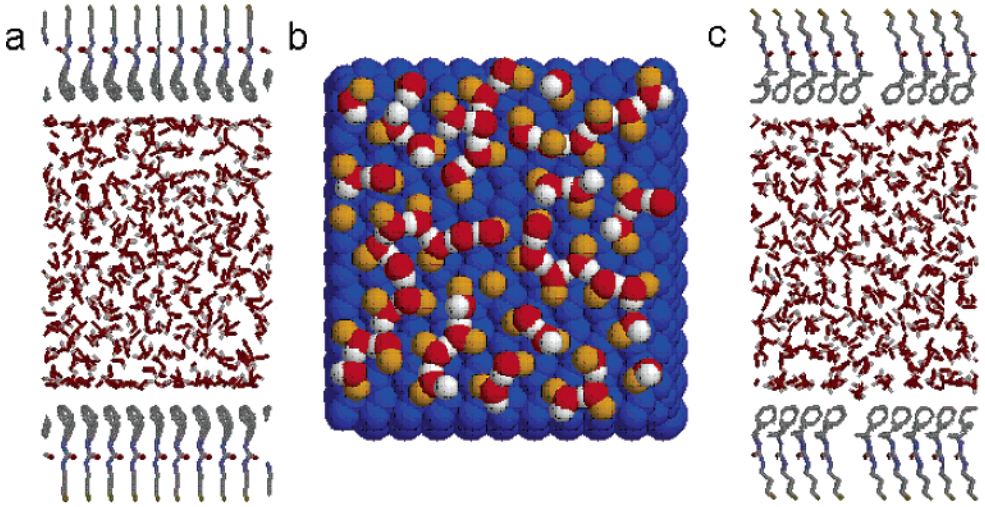

Figure 6. Snapshots from the simulations of methanol between two PEPU surfaces. A side view of the simulation cell is shown in (a), and a snapshot of the contact layer (0−5 Å above the surface) is shown in (b). Each interface is 900 $Å^2$ with 100 PEPU molecules. The surfaces in (c) each have a row of missing PEPU molecules. Oxygen atoms, hydrogen atoms, and methyl groups are red, white, and yellow, respectively. In (b), the atomic positions of the underlying surface are shown in blue.

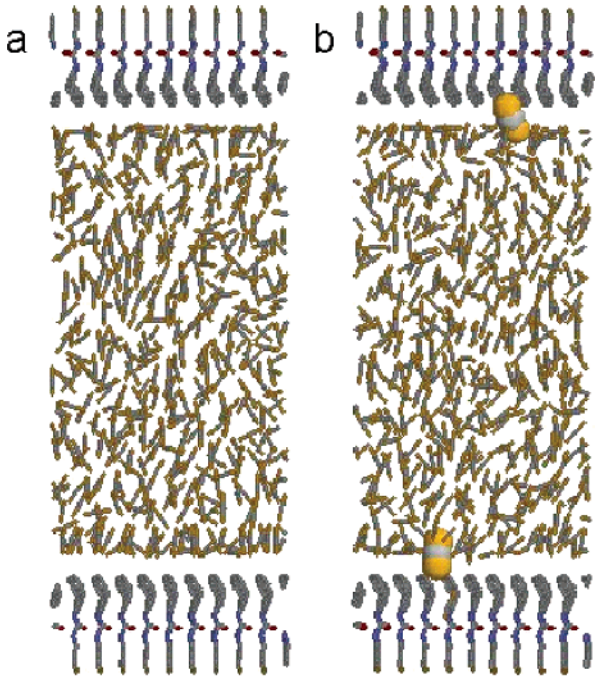

Figure 7. Snapshots from the simulations of CS_2 between two PEPU surfaces. Side views are shown. In (a) the surfaces do not contain imperfections, but five PEPU molecules, which form a cross in the center of the simulated surface, are missing from each surface in (b).

opening (Figure 7b). As with methanol, the CS_2 molecules that descend into the cavity maintain contact with the surface solvent layer.

Overall, the simulations show that the tip−surface interactions will be quite different for water, which forms highly organized layers near the surface. Methanol and CS_2 do form dense layers near PEPU but with less ordering within the solvent surface layer. Imperfections caused by a single surface vacancy did not affect solvent distribution near the surface. Larger imperfections, such as a missing row of PEPU molecules or a five-molecule vacancy, did alter the solvent distribution. Specifically, water enters the cavity formed by five missing PEPU molecules and hydrogen bonds with PEPU molecules around the cavity. Methanol and CS_2 do not fully enter the cross-shaped cavity but choose to maintain contact with the surface layers.

3.4. Selectivity of the PEPU Interface. Force titration profiles for (*R*)- and (*S*)-PEPU-terminated tips on (*R*)- and (*S*)-PEPU-terminated PDMS surfaces in water are shown in Figure 8a. The graph shows the adhesive force interaction observed between tip and sample as a function of pH for each possible *R* and *S* combination. As a control experiment, a force titration profile was also run using the *S* tip on an oxidized (i.e., no PEPU termination) PDMS substrate. The data for the latter experiment are seen in Figure 8b. In both cases, between 300 and 500 force−distance curves were acquired at each pH. Additionally, at any given pH, data were acquired at 10 different points on the surface (the sample being moved several hundred micrometers between each point). The error bars in Figure 8 report the resulting standard deviation in this comprehensive data set (i.e., between 3000 and 5000 force curves) at any given pH. Taking into account the large errors that are observed, it seems there is little evidence for chiral discrimination between tip and sample on the PEPU-terminated PDMS surface. Nor is there any significant pH dependence on the adhesive forces observed. However, a closer analysis of the error data reveals a significant result. Within any single set of data for a given point and pH on the PEPU-terminated PDMS surface, the

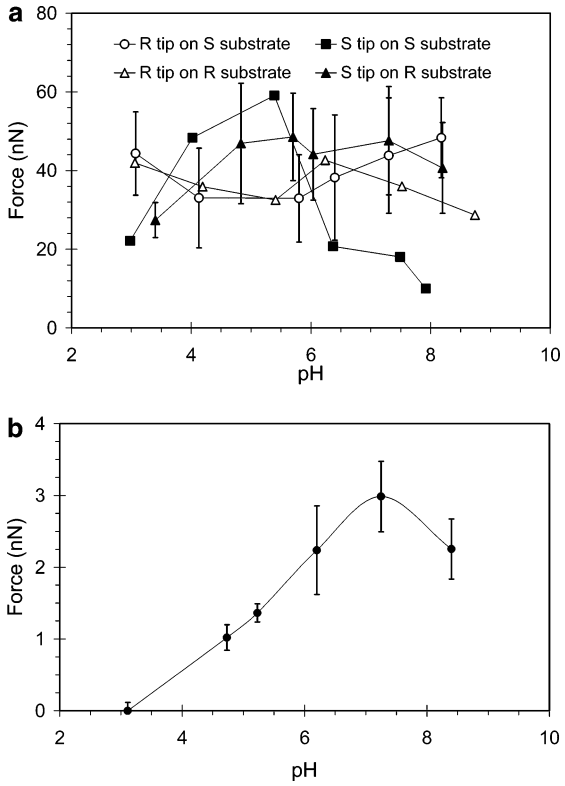

Figure 8. (a) Force titration curves for four different combinations of *R* and *S* isomers of PEPU deposited on an AFM tip and on a PDMS substrate. Note the (typical) error bars shown for the data from the *R*-type tip on the *S*-type substrate. The errors reflect the standard deviation of the data acquired from 300−500 force curves acquired from 10 different locations on the substrate surface. Error bars on the remaining data are similar in magnitude but are omitted for clarity. (b) Force titration curves for a tip coated in the *S* isomer of PEPU on a PDMS surface that had only undergone oxidation using a Tesla coil. Note the much smaller force scale than in (a). The errors reflect the standard deviation of the data acquired from 300−500 force curves at each pH value.

standard deviation is 14%. However, the standard deviation in the average for the 10 points at the same pH is about 3 times as large, at 45%.

The implication of this result, then, is that measurements at any given point of the surface are relatively precise, but that there are real differences in the value of the adhesive interaction observed depending upon the location of the tip, at least on the PEPU-modified PDMS surface. In contrast, similar measurements using the *S*-terminated tip on the oxidized PDMS substrate (Figure 8b) showed no difference in the standard deviation within or between data sets; in other words, this substrate is not site sensitive. This result is perhaps not surprising, in retrospect, since AFM images of this surface show it is extremely rough. Presumably, the tip−sample interaction will be potentially much larger near the bottom of a valley than at the top of the ridge structures. This cannot be tested directly since the PDMS substrate cannot be imaged in contact mode (it is too soft and is readily deformed) but only by using an intermittent-contact mode tip in a separate experiment. The intermittent-contact mode tips have force constants that are too large to obtain good adhesion force data. However, it can be tested indirectly by performing a force titration measurement on a smoother PEPU-terminated surface, such as that formed on the Si(111) substrate. Force titration profiles for (*R*)- and (*S*)-PEPU-terminated tips on (*R*)- and (*S*)-PEPU-terminated silicon surfaces are shown in Figure 9. The variability in the

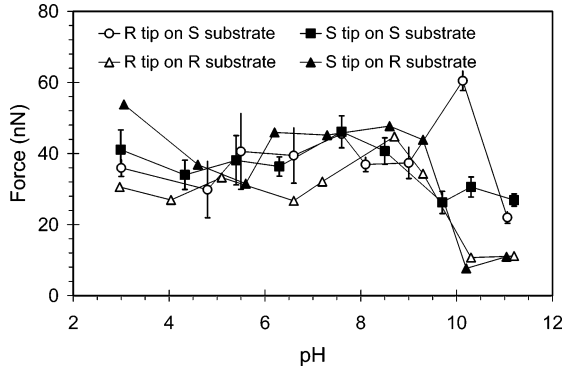

Figure 9. Force titration curves for four different combinations of *R* and *S* isomers of PEPU deposited on an AFM tip and an oxidized Si(111) substrate. Note the (typical) error bars noted for the data from the *R*-type tip on the *S*-type substrate. The errors reflect the standard deviation of the data acquired from 300−500 force curves at each pH value. Error bars on the remaining data are similar in magnitude but are omitted for clarity.

forces observed between the tip and surface in this case was considerably smaller than when using the PDMS substrate. As with the PDMS experiment, 300−500 force curves were acquired at 10 different points on the surface at a given pH. In this case, the average standard deviation within a data set was 6%. The standard deviation between data sets was only 4%. Evidently in this case, the surface is homogeneous enough to have no effect on the force interactions. There appears to be little variation in the magnitude of the adhesive interaction as a function of pH, nor do we see much evidence for chiral selectivity in this system.

Nevertheless, the force titration data observed do give some information. First of all, they indicate that chiral selectivity might be more than just a function of the type of chiral center present: morphology may also play an important role, with a surface containing many configurations of chiral site presumably being less selective. We may also consider the magnitude of the forces observed between the PEPU-modified tip/sample combinations. These range between about 30 and 50 nN, which is of a magnitude similar to that observed for the interaction of a tip and sample coated with self-assembled monolayers of 16-thiohexadecane (60 nN) or 1-thiododecane (12.5 nN).[45,46] This demonstrates that the force interactions observed are dominated by what are commonly referred to as hydrophobic interactions between the PEPU chains. As shown by the molecular dynamics simulations, these large forces arise because, in order to pull apart the tip and sample, the hydrogen bonding water network must be disrupted at the interfacial region. On the oxidized PDMS surface, the largest force observed is much smaller, about 3 nN, and the adhesive interaction is clearly pH dependent, with the largest interactions occurring at high pH. The strong pH dependence must arise due to ionization of the oxidized PDMS surface. Previous results have suggested that the surface pK_a of oxidized PDMS is on the order of 4.0, meaning that at pH values above this the surface will become deprotonated and acquire a significant negative charge. It is on just such a surface that the tip seems to undergo the largest interaction. Evidently, the dominant forces are no longer hydrophobic in nature; otherwise we would expect to see the maximum forces at low pH (where the tip and sample should both show relatively little surface charge). Instead, the result suggests that ionic hydrogen bonds may form under the high pH conditions between Si−O^- sites on the surface and the N−H group of the urea portion of the PEPU-coated tip.

TABLE 3: Adhesive Chemical Force Interactions Observed between (*R*)- and (*S*)-PEPU Terminated Tips and Si(111) Samples in Methanol

tip terminal group	adhesive interaction (nN) on sample		
	(*R*)-PEPU	(*S*)-PEPU	*rac*-PEPU
(*R*)-PEPU	6.7 ± 1.7	1.8 ± 0.5	6.2 ± 3.0
(*S*)-PEPU	2.7 ± 0.7	6.7 ± 2.0	6.7 ± 3.0
rac-PEPU	7.4 ± 2.5	6.6 ± 2.0	6.3 ± 3.0

The experiment on the PEPU-terminated Si(111) surface was repeated, this time using methanol as the solvent. As seen in Table 3, in this case discrimination was indeed observed on the surface, with the like−like (*R*−*R* or *S*−*S*) combination having an interaction about 2 nN greater than the unlike (*S*−*R* or *R*−*S*) combinations. The same tip was used in both pairs of experiments, with 300 data points being collected at four different locations on the surface. The errors reported are the standard deviation from all 1200 data points, although the adhesive wells observed did not vary within experimental error between points on the surface in this case. Using tips coated with a racemic mixture of PEPU resulted in no variation in force interaction on (*R*)- and (*S*)-PEPU-terminated surfaces. Similar experiments were carried out in CS_2, but were unsuccessful, as CS_2 appears to dissolve the PEPU layer on the substrate. Experiments carried out in hexane, a nonpolar but less aggressive solvent, were inconclusive: no adhesive wells were observed, nor was any significant repulsive interaction apparent in the approach portion of the force curves.

In a similar experiment using a tip coated with a Pirkle-type CSP similar in structure to PEPU (DNB-phenylglycine) but a surface consisting of mandelic acid, discrimination was observed in ethanol.[11,47] The forces observed in this case were on the order of 1−2 nN, somewhat smaller than the 2−6 nN we observed in methanol. They are much smaller than those observed in water where no chiral discrimination was seen. However, the *difference* in adhesive interaction between like−like and unlike pairs was similar to the values we find in methanol. We would attribute these differences to two effects. First, for the data acquired in water as a solvent, hydrophobic forces are much more important than in a less polar solvent such as methanol or ethanol. Our system lacks the strongly hydrogen bonding carboxylate groups that are present in mandelic acid. These groups would serve to break up the hydrogen bonding water structures at the surface. Both effects would serve to reduce the strong hydrophobic forces that otherwise overwhelm any small differences in adhesive forces due to chiral discrimination in water. In methanol, the solvent no longer forms strong hydrogen bonding networks in the interfacial region. Furthermore, methanol shows less tendency to interact with the PEPU layer, even when there are defects present. This leaves the chiral centers at the end of the molecules free to interact with one another at the interface and give rise to chiral discrimination.

4. Conclusions

In this article, we have reported a detailed examination of structure, solvation, and selectivity of a type I chiral stationary phase. The selective interface is formed from (*S*)- and (*R*)-*N*-(1-phenylethyl)-*N*′-[3-(triethoxysilyl)propylurea (PEPU) which self-assembles on Si(111) and poly(dimethylsiloxane) (PDMS). Templating PEPU onto these surfaces provides two extremes in surface morphology: The Si(111) interface is smooth whereas PDMS templates a complex surface with broad ridges and deep valleys. Exploration of the PEPU interfaces proceeds with

chemical force measurements, ab initio calculations, and molecular dynamics simulations.

Ab initio results suggest that hydrogen bonding between PEPU molecules maintains and encourages chain (tether) alignment and "stiffens" the PEPU interface. The presence of water, hydroxide, or hydronium ions between the tethers has been explored but always leads to an increase in the intertether distance and disrupts the crucial intertether hydrogen bonding. This suggests that solvent will be excluded, to a large extent, from the intertether region for a dense array of PEPU molecules. On the other hand, the morphology of the PDMS surface, with its numerous ridge and valley features, may accommodate localized tether−solvent interactions. However, the overall solvent−tether interaction should be small since, given the dimensions of typical ridges, only a small fraction of the PEPU molecules will be suitably positioned.

Chemical force measurements of selectivity at the PEPU interface highlight the pivotal role of solvent in surface selectivity. The forces measured for hydrated PEPU surfaces are very large, but discrimination cannot be detected given the standard errors. Methanol, a less polar solvent, gives smaller forces and detectable discrimination. In particular, the homochiral forces are significantly larger than those measured when the PEPU molecules on the surface and tip differ in handedness. An apolar solvent tends to either dissolve the PEPU or lead to repulsive forces.

Molecular dynamics simulations of the solvent−PEPU interface reveal that water forms a highly organized layer near the surface. In particular, water molecules tend to lie flat on the surface while forming rings of hydrogen bonded molecules. Methanol and CS_2 also form dense layers but with considerably less organization within the solvent surface layer. Imperfections caused by a single surface vacancy do not affect solvent distribution near the surface. Larger imperfections, such as a missing row of PEPU molecules or a five-molecule vacancy, did alter the solvent distribution. In particular, water enters the cavity formed by five missing PEPU molecules to hydrogen bond with PEPU molecules around the cavity.

Acknowledgment. The financial support of the Natural Sciences and Engineering Research Council (NSERC) of Canada is gratefully acknowledged.

References and Notes

(1) Wainer, I. W. *Trends Anal. Chem.* **1987**, *6*, 135.
(2) Maier, N. M.; Franco, P.; Lindner, W. *J. Chromatogr., A* **2001**, *906*, 3−33.
(3) Betschinger, F.; Libman, J.; Shanzer, A. *J. Chromatogr., A* **1996**, *746*, 53−62.
(4) Capka, M.; Bartlova, M.; Krause, H. W.; Schmidt, U.; Fischer, C.; Oehme, G. *Am. Biotechnol. Lab.* **1995**, *13*, 13−14.
(5) Dyas, A. M.; Robinson, M. L.; Fell, A. F. *Chromatographia* **1990**, *30*, 73−79.
(6) Lopinski, G. P.; Moffatt, D. J.; Wayner, D. D. M.; Wolkow, R. A. *Nature* **1998**, *392*, 909−911.
(7) Lorenzo, M. O.; Haq, S.; Bertrams, T.; Murray, P.; Raval, R.; Baddeley, C. J. *J. Phys. Chem. B* **1999**, *103*, 10661−10669.
(8) Dodero, G.; De Michieli, L.; Cavalleri, O.; Rolandi, R.; Oliveri, L.; Dacca, A.; Parodi, R. *Colloids Surf. A* **2000**, *175*, 121−128.
(9) Xu, Q.-M.; Wan, L.-J.; Wang, C.; Bai, C.-L.; Wang, Z.-Y.; Nozawa, T., *Langmuir* **2001**, *17*, 6203−6206.
(10) Losic, D.; Shapter, J. G.; Gooding, J. J. *Langmuir* **2002**, *18*, 5422−5428.
(11) McKendry, R.; Theoclitou, Ma.-E.; Rayment, T.; Abell, C. *Nature* **1998**, *391*, 566−568.
(12) Lipkowitz, K. B. *J. Chromatogr., A* **2001**, *906*, 417−442.
(13) Lipkowitz, K. B. *J. Chromatogr., A* **1995**, *694*, 15−37.
(14) Lipkowitz, K. B. *J. Chromatogr., A* **1994**, *666*, 493−503.
(15) Lipkowitz, K. B. *Chem. Rev.* **1998**, *98*, 1829−1873.
(16) Dappen, R.; Karfunkel, H. R.; Leusen, F. J. J. *J. Comput. Chem.* **1990**, *11*, 181.
(17) Lipkowitz, K. B.; Antell, S.; Baker, B. *J. Org. Chem.* **1990**, *54*, 5449.
(18) Still, M. G.; Rogers, L. B. *J. Comput. Chem.* **1990**, *11*, 242.
(19) Aerts, J. *J. Comput. Chem.* **1995**, *16*, 914.
(20) Booth, T. D.; Azzaoui, K.; Wainer, I. W. *Anal. Chem.* **1997**, *69*, 3879.
(21) Wolf, R. M.; Francotte, E.; Lohmann, D. *J. Chem. Soc., Perkin Trans.* **1988**, *2*, 893.
(22) Kohl, D. B.; Patrick, D. L. *J. Phys. Chem. B* **2001**, *105*, 8203−8211.
(23) Ahuja, S. In *Chiral Separations: Applications and Technology*; American Chemical Society: Washington, DC, 1997.
(24) Frisch, M. J.; Trucks, G. W.; Schlegel, H. B.; Scuseria, G. E.; Robb, M. A.; Cheeseman, J. R.; Zakrzewski, V. G.; Montgomery, J. A., Jr.; Stratmann, R. E.; Burant, J. C.; Dapprich, S.; Millam, J. M.; Daniels, A. D.; Kudin, K. N.; Strain, M. C.; Farkas, O.; Tomasi, J.; Barone, V.; Cossi, M.; Cammi, R.; Mennucci, B.; Pomelli, C.; Adamo, C.; Clifford, S.; Ochterski, J.; Petersson, G. A.; Ayala, P. Y.; Cui, Q.; Morokuma, K.; Malick, D. K.; Rabuck, A. D.; Raghavachari, K.; Foresman, J. B.; Cioslowski, J.; Ortiz, J. V.; Baboul, A. G.; Stefanov, B. B.; Liu, G.; Liashenko, A.; Piskorz, P.; Komaromi, I.; Gomperts, R.; Martin, R. L.; Fox, D. J.; Keith, T.; Al-Laham, M. A.; Peng, C. Y.; Nanayakkara, A.; Challacombe, M.; Gill, P. M. W.; Johnson, B.; Chen, W.; Wong, M. W.; Andres, J. L.; Gonzalez, C.; Head-Gordon, M.; Replogle, E. S.; Pople, J. A. *Gaussian 98*, revision A.9; Gaussian, Inc.: Pittsburgh, PA, 1998.
(25) Morra, M.; Occhiello, E.; Marola, R.; Garbassi, F.; Humphrey, P.; Johnson, D. *J. Colloid Interface Sci.* **1990**, *137*, 11−24.
(26) Wang, B.; Abdulali-Kanji, Z.; Dodwell, E.; Horton, J. H.; Oleschuk, R. D.; *Electrophoresis* **2003**, *24*, 1442−1450.
(27) Hines, M. A. *Int. Rev. Phys. Chem.* **2001**, *20*, 645−672.
(28) Hutter, J. L.; Bechhoefer, J. *Rev. Sci. Instrum.* **1993**, *64*, 1868−1873.
(29) McKeehan, L. W. *Phys. Rev.* **1923**, *21*, 503.
(30) Guttman, L.; Rahman, S. M. *Phys. Rev. B* **1988**, *37*, 2657.
(31) Becke, A. D. *J. Chem. Phys.* **1993**, *98*, 5648.
(32) Foresman, J. B.; Keith, T. A.; Wiberg, K. B.; Snoonian, J.; Frisch, M. J. *J. Phys. Chem.* **1996**, *100*, 16098−16104.
(33) MacKerell, A. D., Jr.; Bashford, D.; Bellott, M.; Dunbrack, R. L., Jr.; Evanseck, J. D.; Field, M. J.; Fischer, S.; Gao, J.; Guo, H.; Ha, S.; Joseph-McCarthy, D.; Kuchnir, L.; Kuczera, K.; Lau, F. T. K.; Mattos, C.; Michnick, S.; Ngo, T.; Nguyen, D. T.; Prodhom, B.; Reiher, W. E. III; Roux, B.; Schlenkrich, M.; Smith, J. C.; Stote, R.; Straub, J.; Watanabe, M.; Wiorkiewicz-Kuczera, J.; Yin, D.; Karplus, M. CHARMM. *J. Phys. Chem. B* **1998**, *102*, 3586−3616.
(34) Berendsen, H. J. C.; Grigera, J. R.; Straatsma, T. P. *J. Phys. Chem.* **1987**, *91*, 6269.
(35) Tildesley, D. J.; Madden, P. A. *Mol. Phys.* **1981**, *42*, 1137.
(36) Jorgensen, W. L. *J. Phys. Chem.* **1986**, *90*, 1276−1284.
(37) Hoover, W. G. *Phys. Rev. A* **1985**, *31*, 1695−1697.
(38) Shelley, J. C.; Patey, G. N. *Mol. Phys.* **1996**, *88*, 385.
(39) Ewald, P. P. *Ann. Phys.* **1921**, *64*, 253−287.
(40) Smith, E. R. *Proc. R. Soc. London, A* **1981**, *375*, 475−505.
(41) Yeh, I. C.; Berkowitz, M. L. *J. Chem. Phys.* **1999**, *111*, 3155−3162.
(42) Chaudhury, M. K.; Whitesides, G. M. *Langmuir* **1991**, *7*, 1013−1025.
(43) Hoogboom, J.; Behdani, M.; Elemans, J. A. A. W.; Devillers, M. A. C.; de Gelder, R.; Rowan, A. E.; Rasing, T.; Nolte, R. J. M. *Angew. Chem., Int. Ed.* **2003**, *42*, 1812−1815.
(44) Osterholtz, E. D.; Pohl, E. R. In *Silane and Other Coupling Agents*; Mittal, K. I., Ed.; VSP International Science Publishers: Zeist, The Netherlands, 1992; pp 119−142.
(45) Noy, A.; Vezenov, D. V.; Lieber, C. M. *Annu. Rev. Mater. Sci.* **1997**, *27*, 381−421.
(46) Sinniah, S. K.; Steel, A. B.; Miller, C. J.; Reutt-Robey, J. E. *J. Am. Chem. Soc.* **1996**, *118*, 8925.
(47) McKendry, R.; Theoclitou, M.-E.; Abell, C.; Rayment, T. *Jpn. J. Appl. Phys.* **1999**, *38*, 3901−3907.